BGSG

Volume 56

Research Paper

FIRST RESULTS ON THE M_W=6.9 SAMOS EARTHQUAKE OF 30 OCTOBER 2020

Panayotis Papadimitriou[1*], Vasilis Kapetanidis[1], Andreas Karakonstantis[1], Ioannis Spingos[1], Ioannis Kassaras[1], Vassilis Sakkas[1], Vasiliki Kouskouna[1], Anna Karatzetzou[2], Kyriaki Pavlou[1], George Kaviris[1], Nicholas Voulgaris [1]

[1] Section of Geophysics-Geothermics, Department of Geology and Geoenvironment, ppapadim@geol.uoa.gr, vkapetan@geol.uoa.gr, akarakon@geol.uoa.gr, ispingos@geol.uoa.gr, kassaras@geol.uoa.gr; vsakkas@geol.uoa.gr; vkouskouna@geol.uoa.gr; kpavlou@geol.uoa.gr; gkaviris@geol.uoa.gr; voulgaris@geol.uoa.gr

National Kapodistrian University of Athens, Panepistimiopolis 15784, Athens, Greece

[2] Department of Civil Engineering, Aristotle University of Thessaloniki, University Campus 54636, Thessaloniki, Greece akaratze@civil.auth.gr

Correspondence to:
Panayotis Papadimitriou
ppapadim@geol.uoa.gr

DOI number:
http://dx.doi.org/10.12681/bgsg.25359

Keywords:
Earthquake, Seismotectonics, aftershocks, Coulomb stress transfer, deformation, shakemap

Citation:
Papadimitriou P., Kapetanidis V., Karakonstantis A., Spingos I., Kassaras I., Sakkas V., Kouskouna V., Karatzetzou A., Pavlou K., Kaviris G. and Voulgaris N. (2020), First Results on the M_w=6.9 Samos Earthquake of 30 October 2020. Bulletin Geological Society of Greece, 56, 251-279.

Publication History:
Received: 20/11/2020
Accepted: 26/11/2020
Accepted article online: 28/11/2020

The Editor wishes to thank Efthimios Sokos for his work with the scientific reviewing of the manuscript and Ms Emmanouela Konstantakopoulou for editorial assistance

Abstract

On 30 October 2020 11:51 UTC, a M_w=6.9 earthquake struck the offshore region north of Samos Island, Greece, in the Gulf of Ephesos/Kuşadasi, causing two fatalities and 19 minor injuries at Samos Island, as well as 115 casualties and over 1,030 injuries in Western Turkey. Preliminary results indicate that the mainshock occurred on a north-dipping normal fault, with a focal mechanism of 270°/50°/-81°. The selection of the fault plane is supported by evidence of uplift at western Samos and over 10 cm of subsidence at the northernmost edge of the central part of the island. The distribution of relocated hypocenters shows clustering of events, east of the mainshock's epicenter, where most major aftershocks have occurred. To the west, a smaller group of aftershocks is observed, separated by a spatial gap in seismicity. The latter is likely related to the region of the fault plane where most of the co-seismic slip occurred, with Coulomb stress-transfer towards the western and eastern margins of the rupture triggering aftershock activity. The apparent complexity of the mainshock's source time function, supported by preliminary results, could indicate the rupture of more than one structures. This could explain the relatively weak magnitude of the largest aftershock (M_w=5.0). The mainshock caused damage mainly to non-engineered constructions, i.e. old residential buildings, churches and monuments in Samos Island, and minor damage to the majority of the building stock of the island built according to the National Seismic Code. On the other hand, it caused severe damage at Izmir, especially to high-rise

buildings. The mainshock also triggered a small tsunami that reached heights of over 1 m, mainly affecting the Turkish coast.

Keywords: *Earthquake, Seismotectonics, aftershocks, Coulomb stress transfer, deformation, shakemap*

Περίληψη

Στις 30 Οκτωβρίου 2020 11:51 UTC (τοπική ώρα 13:51) εκδηλώθηκε ένας σεισμός μεγέθους M_w=6.9 στην παράκτια ζώνη βόρεια της Σάμου, στον Κόλπο της Εφέσου / Kuşadasi, προκαλώντας δύο ανθρώπινες απώλειες και 19 ελαφριούς τραυματισμούς στη νήσο Σάμο, ενώ αναφέρθηκαν 115 θάνατοι και πάνω από 1.030 τραυματισμοί στη Δυτική Τουρκία. Προκαταρκτικά αποτελέσματα υποδεικνύουν ότι ο κύριος σεισμός έλαβε χώρα σε ένα κανονικό ρήγμα με κλίση προς Βορρά, με παραμέτρους μηχανισμού γένεσης 270°/50°/-81°. Η επιλογή του επιπέδου διάρρηξης υποστηρίζεται από ενδείξεις ανύψωσης στο δυτικό τμήμα της νήσου Σάμου, το οποίο ανήκει στο ανερχόμενο τέμαχος και πάνω από 10 cm καθίζησης στη βορειότερη άκρη του κεντρικού τμήματος του νησιού. Η κατανομή των επαναπροσδιορισμένων υποκέντρων αναδεικνύει σχηματισμό συστάδων γεγονότων ανατολικά του επικέντρου του κύριου σεισμού, όπου έχουν εκδηλωθεί οι περισσότεροι μετασεισμοί, ενώ δυτικά του κύριου σεισμού παρατηρείται μια μικρότερη ομάδα μετασεισμών, η οποία διαχωρίζεται από ένα κενό στο οποίο εντοπίζονται ελάχιστα γεγονότα. Το τελευταίο πιθανόν συνδέεται με μια περιοχή του επιπέδου διάρρηξης όπου σημειώθηκε η ισχυρότερη ολίσθηση, με μεταφορά τάσης Coulomb προς τα δυτικά και ανατολικά άκρα της να προκαλεί μετασεισμική δραστηριότητα. Η πολυπλοκότητα της χρονικής συνάρτησης σεισμικής πηγής του κύριου σεισμού, όπως παρατηρήθηκε σε προκαταρκτικά αποτελέσματα, υποδεικνύει ότι πιθανόν η κύρια διάρρηξη να εμπλέκει περισσότερες από μια ενεργές δομές, κάτι που πιθανόν εξηγεί το χαμηλό μέγεθος του μεγαλύτερου μετασεισμού (M_w=5.0). Ο κύριος σεισμός προκάλεσε βλάβες κυρίως σε κατασκευές χωρίς αντισεισμικό σχεδιασμό, δηλαδή σε παλιές κατοικίες, εκκλησίες και μνημεία στη νήσο Σάμο, και ελαφρές βλάβες στην πλειονότητα του κτηριακού αποθέματος του νησιού το οποίο έχει κατασκευαστεί σύμφωνα με τις προδιαγραφές του Εθνικού Αντισεισμικού Κανονισμού. Από την άλλη, προκάλεσε σοβαρές βλάβες στη Σμύρνη, κυρίως σε υψηλά κτήρια. Ο κύριος σεισμός προκάλεσε επίσης ένα μικρό τσουνάμι, το οποίο ξεπέρασε σε ύψος το 1 m, κυρίως στις ακτές της Τουρκίας.

Λέξεις-κλειδιά: *Σεισμός, σεισμοτεκτονική, μετασεισμοί, μεταφορά τάσης Coulomb, παραμόρφωση, χάρτης ισχυρής εδαφικής κίνησης*

1. INTRODUCTION

The Aegean Sea is one of the most seismically active areas in the SE Mediterranean. The western extension of the North Anatolian Fault, to the north, and the Hellenic Trench, to the south, bound the Aegean microplate (McKenzie, 1978; Mercier *et al.*, 1989). Tectonics in the northern Aegean are dominated by dextral strike-slip faulting along NE-SW striking structures, parallel to the North Aegean Trough, while conjugate sinistral strike-slip faulting is also present, associated with certain large events (e.g. the 26 July 2001 *M*=6.3 and the 3 April 1967 *M*=6.7 earthquakes near Skyros Island; McKenzie, 1972; Karakostas *et al.*, 2003; Roumelioti *et al.*, 2003). The tectonic environment around the eastern Aegean strongly differs; E-W striking faults close to the Greek islands (such as Samos) and the Western Turkish shores exhibit oblique-normal motions. These localized systems are closely related to minor basins and gulfs around the Greek-Turkish border, as in the cases of Lesvos-Edremit (Kurtuluş *et al.*, 2009), Samos-Kuşadasi (Tan *et al.*, 2014) and Gökova (Gürer *et al.*, 2013).

The broader area of the eastern Aegean Sea (Fig. 1) is part of a zone where transitions between extension and shear deformation are observed, ranging in width about 100 km (e.g. Papazachos, 1999). GPS measurements indicate that the anomalously slow extension rate, compared to the elevated values that prevail in the rest of the Aegean, allows the Anatolia microplate to move with increasing velocity to the WSW, leading to the westward opening of the Izmir Bay (e.g. Mascle and Martin, 1990). The deformation that occurs at the onshore part of western Turkey features N-S trending crustal extension, evidenced by numerous earthquakes located along the Inner İzmir Bay Basin and the Gulf of Ephesos/Kuşadasi (Genç *et al.*, 2001). Nevertheless, there are also scarce occurrences of strike-slip faulting in the broader area of Karaburun peninsula (e.g. Ocakoğlu *et al.*, 2004), including the 2005 Sigacik sequence north of Samos Island (Benetatos et al., 2006).

Samos is a largely mountainous Greek island, approximately 1.5 km away from the Turkish shore in the east. It hosts several areas of economic interest, such as Karlovasi to the northwest and Vathy (also named “Samos”) to the northeast (Fig. 2). The island's population is 33,814, which makes it the 9th most populous of the Greek islands. Samos’ mountains are an extension of the Mycale range on the Anatolian mainland. The geology of the island consists of several metamorphic nappes, a non-metamorphic nappe and a Miocene graben. Because of the quite complicated geology (Fig. 2), the island offers a look on an exceptionally complete nappe stack of the Central Hellenides, ranging from the high-pressure metamorphic Basal Unit (as part of the External

Hellenides) all the way up to the ophiolitic Sélcuk nappe and the non-metamorphic Cycladic ophiolite nappe (Pomonis & Hatzipanagiotou, 1998; Ring *et al.*, 2007; Jolivet & Brun 2010; Malandri *et al.*, 2017).

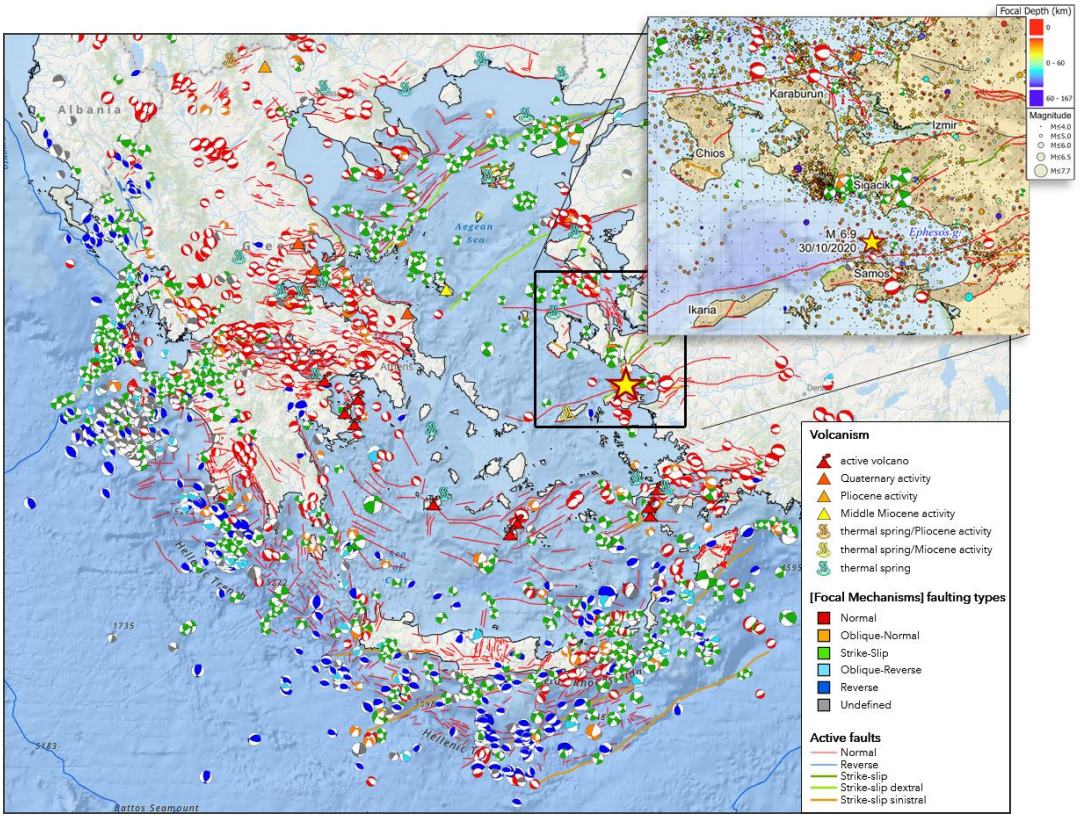

Fig. 1: Snapshot from the New Seismotectonic Atlas of Greece v1.0 (Kassaras *et al.*, 2020), presenting focal mechanisms (period 1995 – June 2020, by SL-NKUA) and active faults (NOAFAULTs, Ganas *et al.*, 2018), coloured by faulting type, along with volcanism and hydrothermal activity. The epicenter of the October 30th 2020 mainshock is presented by a yellow star. Inset map: past instrumental seismicity (1901-June 2020; from the compilation of Kassaras *et al.*, 2020) and focal mechanisms of significant earthquakes at crustal depths (from the compilation of Kapetanidis & Kassaras, 2019) in the broader region of the 2020 Samos earthquake. The interactive GIS web application of the New Seismotectonic Atlas of Greece v1.0 is available at the following link: http://www.geophysics.geol.uoa.gr/atlas.html

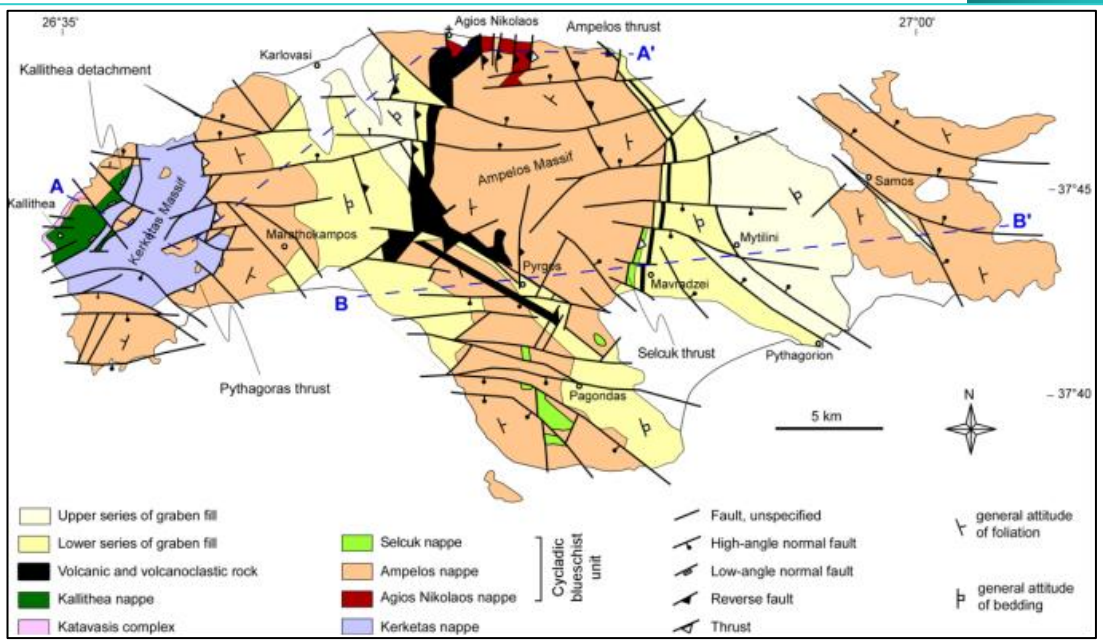

Fig. 2: Geologic map of Samos Island (modified by Ring *et al.*, 2007)

On 30 October 2020 11:51 UTC, a M_w=6.9 earthquake occurred in the offshore area north of Samos Island, in the Gulf of Ephesos/Kuşadasi (Fig. 1). Two fatalities and 19 minor injuries were reported at Samos Island, along with several injuries and significant damage to the building stock. In Western Turkey, the effects of the event were detrimental, with 115 fatalities, over 1,030 injuries and structural damage that included collapses. A minor tsunami was also reported. In this report, we present preliminary results of the mainshock's source parameters and the spatiotemporal distribution of its aftershock sequence, along with the triggering mechanism due to stress redistribution and the observed deformation on Samos Island.

2. PAST SEISMIC ACTIVITY IN THE REGION – HISTORICAL DATA

The seismic history of Samos dates back to the 2nd century BC. Around 201-197 BC, an earthquake caused injuries among the people of the island of Samos. Over 200 years later, circa 46-47 AD, according to an inscription from Samos, in AD 47 the emperor Claudius restored the temple of Dionysus, which had collapsed because of age and an earthquake (Ambraseys, 2009). Until the 18th century, no records on earthquake activity have been reported from Samos. Between 1700 and 1799, eight damaging earthquakes with epicentres in the eastern Aegean affected the island. Particularly the 18 June 1751 event destroyed many houses in the eastern part and in the Turkish region of Kusadasi, causing great losses.

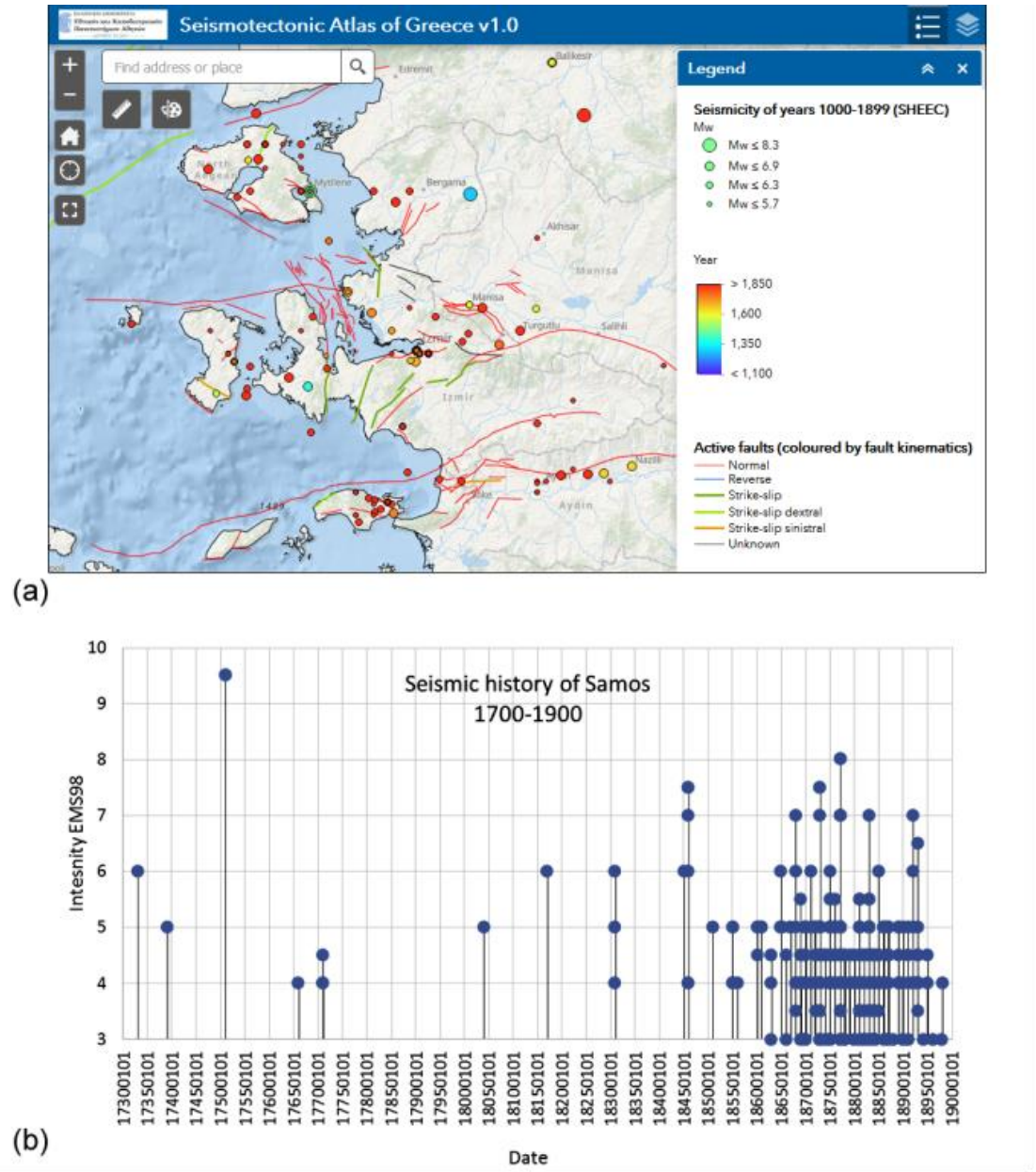

Fig. 3: (a) Epicentral distribution of historical earthquakes with $M_w \geq 5.0$ in the broader Samos area during the period 1000-1899 (Locati *et al.*, 2014), from the New Seismotectonic Atlas of Greece (Kassaras et al., 2020; http://www.geophysics.geol.uoa.gr/atlas.html). Lines show active faults (Ganas *et al.*, 2018). (b) The seismic history of Samos in the period 1700-1900, in terms of assigned EMS98 intensity (Taxeidis, 2003; Kouskouna and Sakkas, 2013).

In the 19th century, ample information on seismicity is retrieved from the contemporary press (Taxeidis, 2003). A total of 416 earthquakes were reported as damaging or felt in Samos (Kouskouna and Sakkas, 2013; Fig. 3b). Structural damage and partial collapse of buildings (intensity of VII) was caused by 14 of these events, mainly in the second half of the century. Furthermore, 11 events produced non-structural damage (intensity between VI and VII), with the rest being strongly felt with negligible damage. The parameters of these earthquakes are assessed in many parametric catalogues (Papazachos and Papazachou, 2003; Taxeidis, 2003; Stucchi *et al.*, 2013), mainly based on macroseismic intensity data distribution inversion techniques, e.g. the "boxer" method by Gasperini *et al.* (2010) in the SHEEC catalogue of Stucchi *et al.* (2013). The distribution of macroseismic data points, as well the epicentre of each earthquake, are included in the Hellenic Macroseismic database (Kouskouna and Sakkas 2013; http://macroseismology.geol.uoa.gr/query_eq/) and the AHEAD database (Locati *et al.*, 2014; Fig. 3a).

The historical earthquakes magnitudes have been estimated in equivalent moment magnitude (M_w) using macroseismic data. For the events with more than 10 macroseismic intensity data points, the "Boxer" method was applied (Gasperini *et al.*, 2010) and for those with fewer intensity data points a local empirical relationship was used (Taxeidis, 2003). The estimated magnitudes were found in the range of 3.9-7.3 (Fig. 3a), with 46 events having magnitudes greater than 5.0. The magnitude uncertainties of such estimations may reach the value of ±0.5. In the early 20th century, an earthquake on 11 August 1904 (Fig. 4) with estimated equivalent moment magnitude M_w=6.1, is considered the most damaging event in Samos. The mainshock and its largest aftershocks caused severe damages to residential areas and monasteries, which included over 208 collapses, irreparable damages to public infrastructure and four fatalities. Damage in the north part of the island at Karlovasi and lower Vathy was minor with only one house collapsed and 50 damaged.

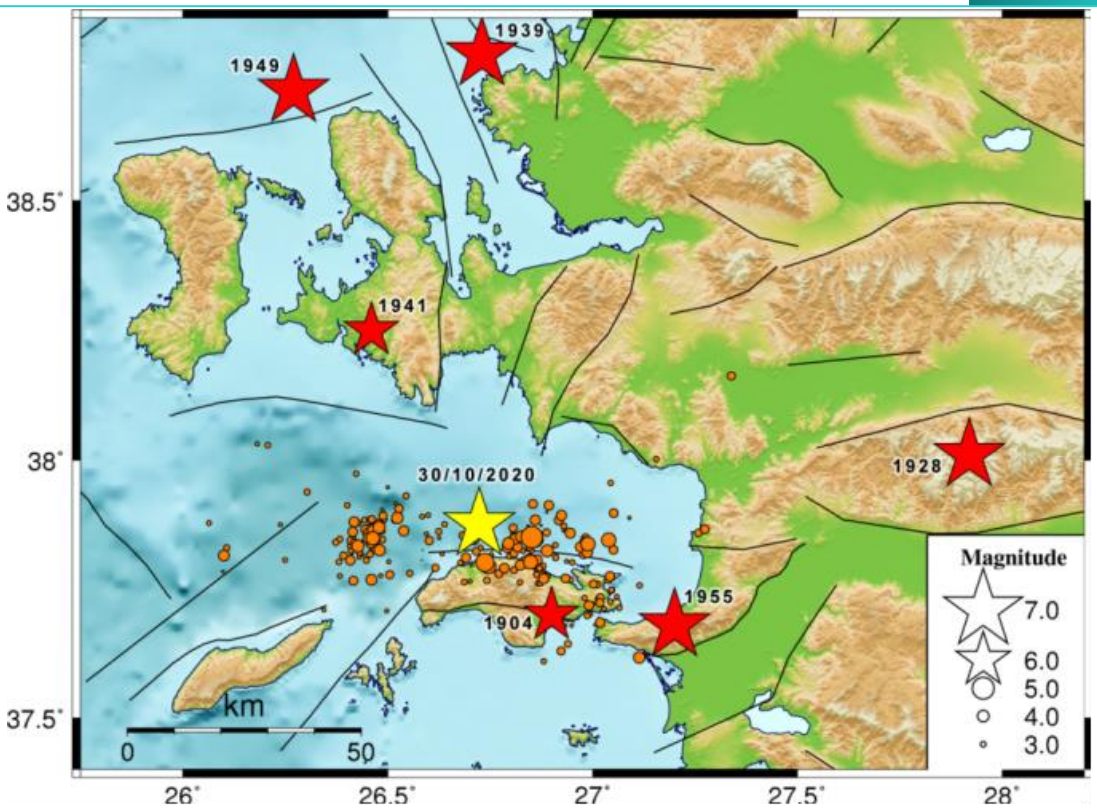

Fig. 4: Epicenter of the October 30th mainshock (yellow star) and large events ($M_w \geq 6.0$) of the instrumental era (red stars) of the broader area of study (from the catalogue of Makropoulos *et al.*, 2012). Orange circles depict the manually located epicenters of the 2020 Samos aftershocks. Lines are the traces of fault sources from the European Database of Seismogenic Faults (EDSF, Basili *et al.*, 2009; Woessner *et al.*, 2015).

3. MATERIALS AND METHODS

During the period between 30 October 2020 and 8 November 2020 a total of 232 events of the 2020 Samos sequence were detected and manually analysed at the Seismological Laboratory of the National and Kapodistrian University of Athens (SL-NKUA) using real-time waveform data from the Hellenic Unified Seismological network (HUSN). We also collected catalogue and arrival-time data from the Geodynamics Institute of the National Observatory of Athens (GI-NOA) and compiled a merged catalogue of 367 events. In addition, we incorporated P and S arrival-time data for these events from stations installed in Turkey, as reported in the bulletin of the Turkish Disaster and Emergency Management Presidency (AFAD; https://deprem.afad.gov.tr). To improve the earthquake catalogue we relocated the hypocenters using the double-difference method HypoDD (Waldhauser, 2001), incorporating both catalogue and cross-correlation travel-time data.

Regarding the determination of focal mechanisms for the mainshock and its major aftershocks, we adopted a processing scheme which uses regional moment tensor inversion. First, suitable waveforms were selected based on a weak noise content, from stations that provide the narrowest possible azimuthal gap. Pre-processing of signal data included the removal of instrument response and their integration to displacement. Next, Green functions were computed with the frequency-wavenumber integration method (Bouchon, 1979, 2003). Synthetic waveforms were then generated and compared with the observed ones, following the procedure proposed by Papadimitriou *et al.* (2012), applying a Butterworth bandpass filter in the frequency range 0.01 Hz – 0.125 Hz. Corrections are iteratively performed to the initial focal mechanism model, until the one providing the minimum misfit is found. The aforementioned method has been successfully applied in several case studies in Greece, e.g. Santorini during the 2011-2012 seismic crisis (Papadimitriou *et al.*, 2015; Kaviris *et al.*, 2015), Lesvos Island, where a normal fault was activated in 2017 (Papadimitriou *et al.*, 2018) and Zakynthos Island, where a low-angle strike-slip fault generated an M_w=6.7 mainshock (Papadimitriou *et al.*, 2020a).

In an initial attempt to study the co-seismic ground deformation caused by the main event, interferometric processing was performed. Satellite radar images from the SENTINEL 1A and 1B constellation were processed using ESA's platform "geohazards TEP" (https://geohazards-tep.eu/). The SNAP algorithm was adopted for the differential interferometric processing. Two pairs of radar images were processed, one on *ascending* and the other on *descending* orbital geometry. For the *ascending* orbital geometry, the time span for the two radar images was 6 days: 24 to 30 October, with an incident angle of ~36.8°. The slave image (30 October) was acquired just few hours after the main event. As a result, the observed deformation describes mainly the co-seismic motion and not contingent post-seismic effects. For the *descending* orbital geometry, the time span was 12 days: 24 October to 5 November.

Lastly, to examine the possible triggering mechanism for the aftershocks by stress redistribution due to the mainshock, we constructed a simplified preliminary model of Coulomb stress transfer using the Coulomb 3.3 software (Toda et al., 2011), by considering a typical fault model based on the total moment magnitude, focal mechanism and observations of deformation for its dip direction and placement.

4. RESULTS

4.1. Focal mechanisms

Based on the above-mentioned methodology for focal mechanism determination by regional body-wave modeling, the source parameters of both the mainshock and the major aftershocks of the sequence were acquired. For the main event, a quite satisfactory fault-plane solution has been obtained (Fig. 5), considering preliminary results by agencies such as USGS (2020) and Geoscope (2020), which indicate a complex source time function (at least two sources). Thus, teleseismic modeling will be required for more information concerning the complexity of the source time function and possible directivity characteristics. The mainshock, with a centroid depth of 13.0 km, produced seismic moment equal to M_0=2.81·10^{26} dyn·cm. Thus, the moment tensor inversion yielded a moment magnitude of M_w=6.9. The determined focal mechanism indicates normal faulting with the fault plane oriented in an almost E-W direction (φ_1=270º, δ_1=50º, λ_1=-81º and φ_2=76º, δ_2=41º, λ_2=-101º, where φ is the strike, δ the dip and λ the rake of each nodal plane, respectively).

Following the mainshock, 28 large aftershocks with $M_w \geq 3.7$ were processed to determine their focal mechanisms (Fig. 6). Initial solutions were estimated by an automated version of the method used to obtain the mainshock's parameters. Each automatic solution is manually revised and the results are published online (www.geophysics.geol.uoa.gr). The focal mechanism of the largest aftershock that occurred a few hours after the main event (30 October 2020 15:14:57 UTC), with M_w=5.0, resembles that of the mainshock, i.e. φ_1=264º, δ_1=37º, λ_1=-126º with a centroid depth of 15.0 km. The average source parameters for the aftershocks, as determined from the distribution of strike, dip and rake angles, seem to agree with the modeling results for the mainshock, indicating E-W to WNW-ESE, almost pure dip-slip normal faulting. To obtain a preliminary estimate of the stress state related to the sequence, we employed the fast stress inversion method of Vavryčuk (2014), which performs iterative joint inversions of stress and fault orientations. The parameters of the principal stress axes for the optimal stress tensor were estimated: $\mathbf{S}_1$ (trend/plunge: *304º/85º*), $\mathbf{S}_2$ (*104º/4º*) and $\mathbf{S}_3$ (*194º/2º*), with an expected focal mechanism for optimally oriented faults with parameters φ_1=287º, δ_1=54º, λ_1=-85º for the north-dipping nodal plane and φ_2=99º, δ_2=36º, λ_2=-97º for the south-dipping one. These results are in agreement with the data-driven stress model produced by Kapetanidis and Kassaras (2019) for the area (east of Samos Island, in particular), insinuating that fault kinematics of the current seismic sequence are consistent with those expected for a north-dipping fault plane,

given the regional stress regime as determined from the focal mechanisms of past earthquakes.

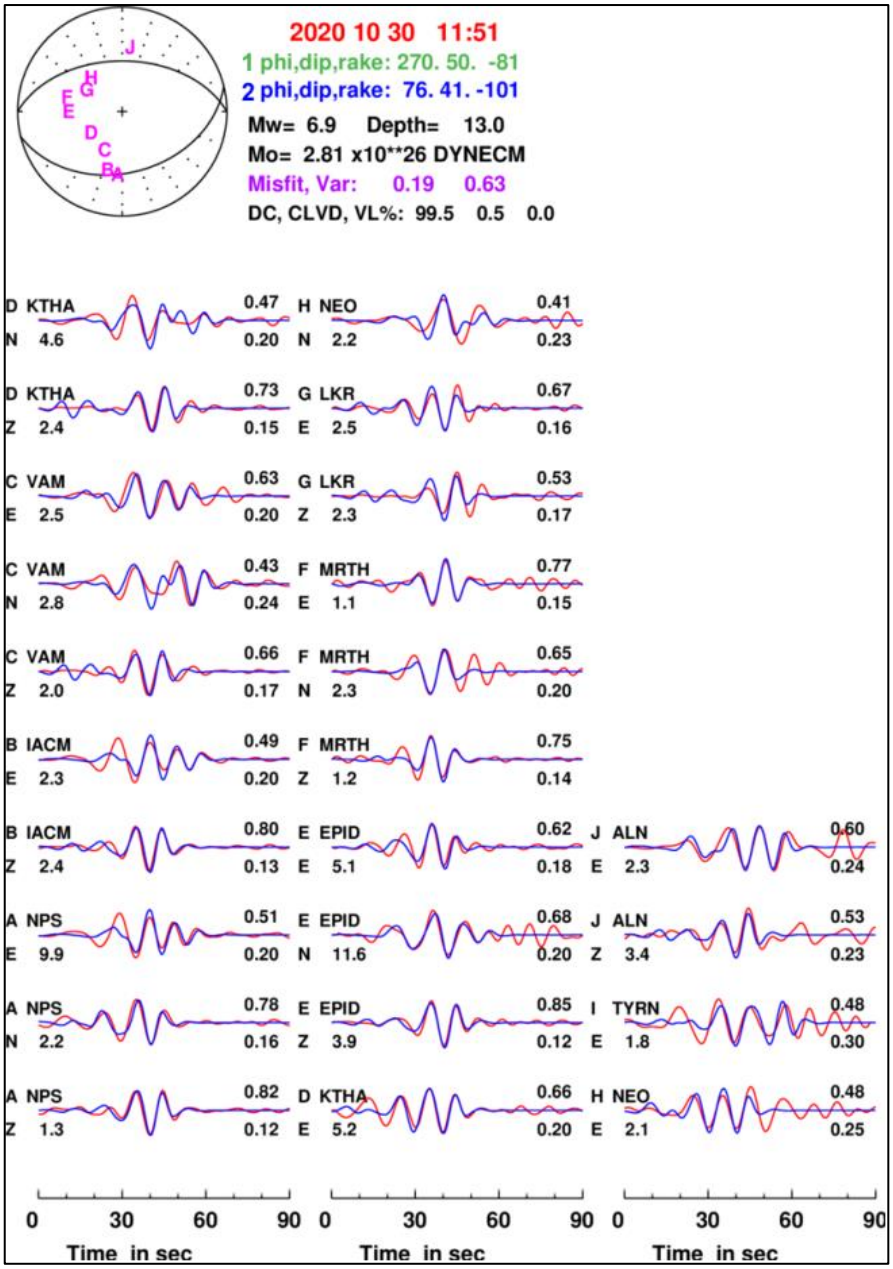

Fig. 5: Results of the focal mechanism determination for the mainshock. The focal mechanism (top), along with key information (including two quality criteria, i.e. the misfit and variance reduction) about the solution are shown. The comparison between observed (red) and synthetic (blue) waveforms is also presented, offering further insight about the reliability of the solution. For each waveform subfigure, the following information is shown (clockwise from top left); the position of the station on the focal sphere (A-J), the station code, the variance reduction, the misfit, the individual seismic moment (in units of 10^{26} dyn·cm) and the component code (i.e. Z for vertical, E for E-W and N for N-S).

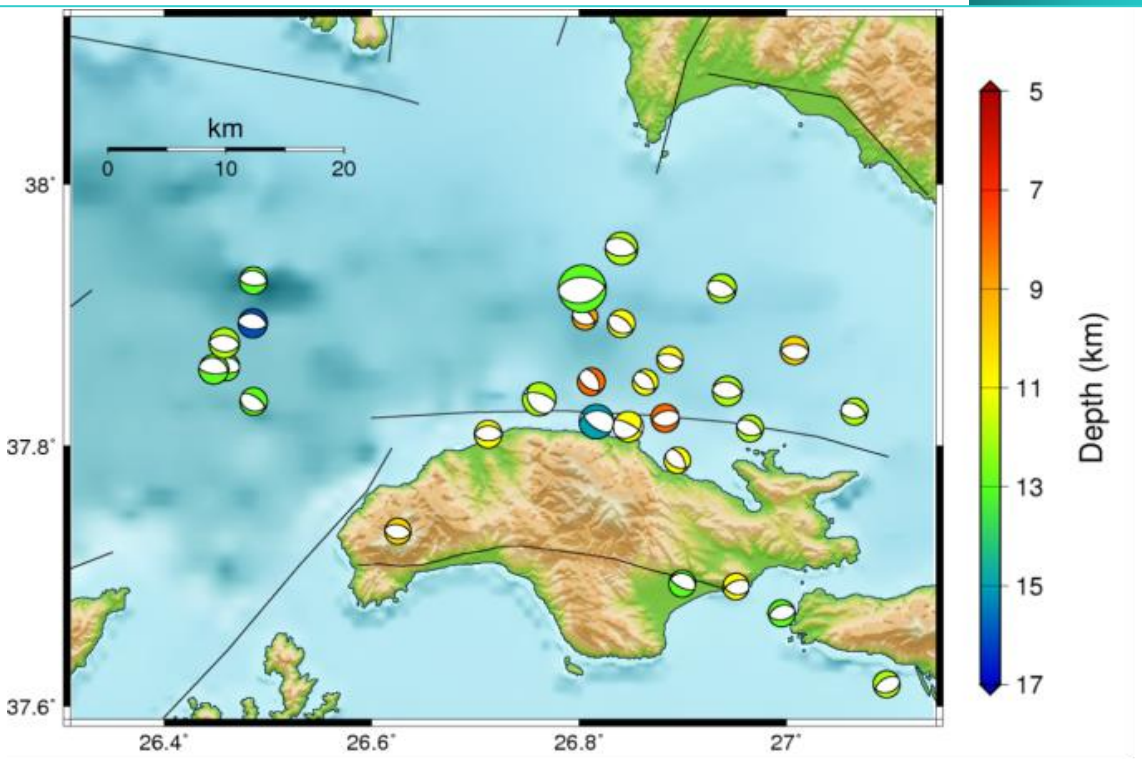

Fig. 6: Focal mechanisms of the 2020 Samos mainshock and 28 major aftershocks ($M_w \geq 3.7$). Beachball locations are from the preliminary epicentral locations of routine analysis.

4.2. Ground deformation

The phase of the differential interferograms was unwrapped and the Line Of Sight (LOS) displacement maps were produced (Fig. 7), presenting the ground displacement in metric units (m). For both orbital geometries, the LOS displacement maps indicate that intense deformation occurred mainly in the northern and western part of the island, i.e. the areas closer to the mainshock's epicentre, while the eastern part exhibits quite smaller amplitudes of LOS displacement. The most prominent feature of the observed deformation is the intense positive LOS displacement values in the western part of the island (motion towards the satellite) for both acquisition geometries. The latter is consistent with the normal faulting motion of the uplifted footwall in the activated seismic fault, taking into consideration that the main motion component of the LOS vector is the vertical one and both geometries resulted to similar positive LOS displacement values. Nevertheless, there is a narrow coastal zone in the northern central part of the island where increased negative LOS displacement values (<-10 cm; motion away from the satellite) were observed. Moreover, the ascending acquisition geometry revealed a different type of motion at the eastern part of Samos with significantly smaller and negative LOS displacement values, indicating a differential motion

between the eastern and western part of the island. However, this is not the case for the descending orbital geometry, where in the eastern part the LOS displacement is significantly smaller compared to the western one, but the values retain a positive sign.

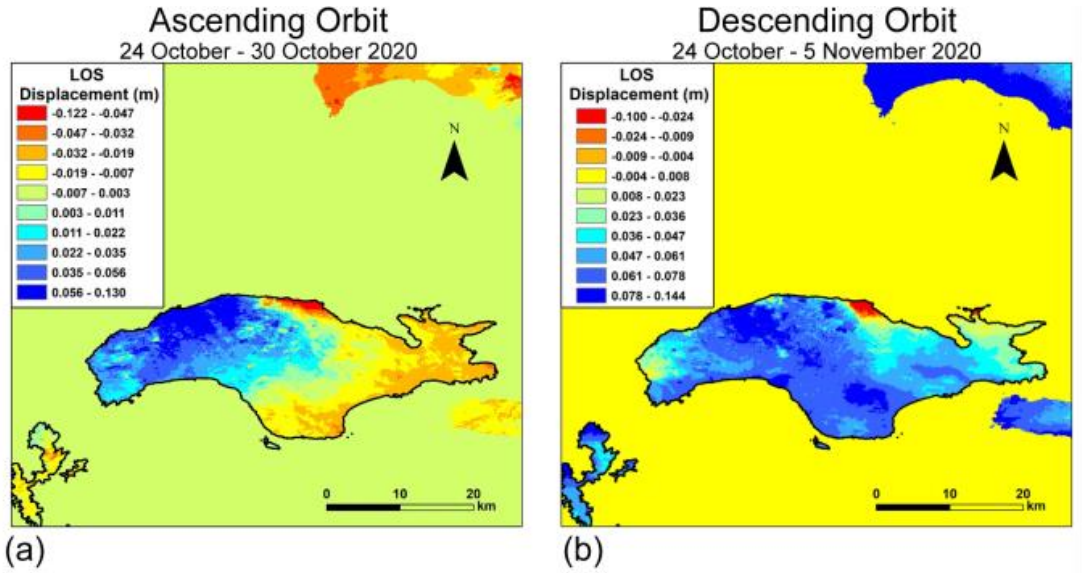

Fig. 7: LOS Displacement maps of Samos Island deduced from interferometric processing of SENTINEL 1A and 1B radar images (a) for *ascending* orbit (24 – 30 October, 2020) and (b) for *descending* orbit (24 October – 5 November, 2020).

It must be stated that the overall deformation image of the island reveals a kinematic discontinuity in the central part of Samos. This feature differentiates the co-seismic motion between the western part (with high positive LOS displacement values) and the eastern part (quite smaller and even negative LOS displacement values in the ascending orbital geometry). Further investigation of the local tectonics and numerical modelling of the seismogenic fault is required to explain this phenomenon, associated with the tectonic status of the area.

4.3. Relocation and spatiotemporal analysis of the aftershock sequence

We initially located the hypocenters using the HypoInverse code (Klein, 2002) and a custom velocity model that was constructed for this sequence (Table 1), determined using the VELEST algorithm (Kissling et al., 1994), starting with a 1D model for the region of Karaburun (Erythres), Turkey (Karakonstantis, 2017). The average V_p/V_s ratio was estimated equal to 1.74, which yielded a minimum average RMS error of 0.37

s. Average horizontal and vertical location errors were estimated as ERH=0.42 km and ERZ=1.74 km, respectively, with the nearest station at a distance of less than 30 km for most events, with a median of ~62 P or S arrival-times per event at ~38 stations, after the incorporation of data from stations installed in Turkey. Although the aftershocks were located at the eastern margins of HUSN, the integration of data from stations located at Turkey achieved a satisfactory average azimuthal gap of 68°, with less than 100° for most events. However, the lack of data from local stations, especially during the first days of the sequence, limited the capability to constrain focal depths and resolve the geometries of the activated structures from the distribution of hypocenters. Furthermore, this caused foci locations to be strongly biased by the selection of the velocity model, which could only be considered as preliminary.

To improve the relative locations of hypocenters, we have relocated the sequence using the HypoDD code (Waldhauser, 2001). This algorithm reduces uncertainties caused by discrepancies between the 1D velocity model and the real structure by minimizing the double difference between calculated and observed travel-times for pairs of neighboring events.

Table 1: Custom 1D P-wave velocity model constructed for the Samos 2020 sequence.

V_P (km/s)	**Ceiling Depth** (km)
5.88	0.0
5.93	11.5
7.13	23.5
7.30	56.5
7.90	82.5

To this purpose, we also incorporated waveform cross-correlation data from available stations in the region. Fig. 8 presents the preliminary relocation results. During the first days of the sequence, local data were mainly available from the accelerometric station KRL1, while data from the permanent station SMG and the temporary stations SAM1 and SAM2 of GI-NOA were available for events that occurred after a few days, in early November 2020. Waveform data from stations at the coasts of Turkey were also incorporated for the relocation procedure.

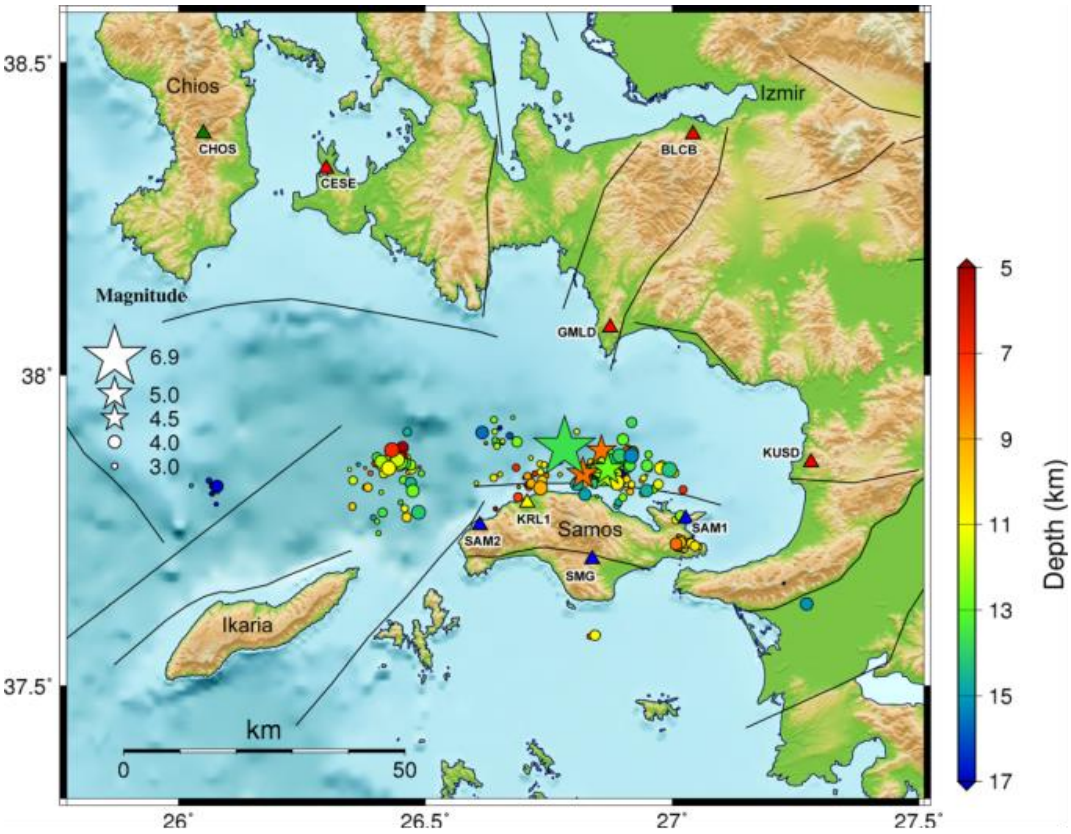

Fig. 8: Preliminary relocation of the 2020 Samos aftershock sequence for the period between 30 October and 8 November 2020. The locations of available stations in the region are presented by triangles (Network codes: blue=HL, yellow=HI, green=HT, red=KO). The major events with M ≥ 4.5 are depicted by stars.

The preliminary results for the 2020 aftershock sequence reveal the existence of several distinct spatial clusters (Fig. 9). The epicenter of the mainshock is located about 10 km N of Samos Island. A dense cluster of aftershocks (group 1, red) has occurred east of the mainshock. This is associated with the major aftershocks ($M_w \geq 4.5$, stars in Fig. 9) that have been reported for this sequence. The largest aftershock was clustered in group 1. An approximately 20-km-long area with very sparse to no seismicity can be observed west of the mainshock, with only few aftershocks in group 2 (green). Further west, a significant cluster of events is observed (group 3), while two additional, smaller, isolated clusters were also located, one at the eastern tip of Samos Island (group 4, cyan) and another to the north of Ikaria Island (group 5, yellow). Cross-sections were performed in both a S-N (Fig. 10, a_1-a_2, b_1-b_2) and a W-E direction (c_1-c_2) to depict the distribution of hypocenters at depth. Most seismicity is in a range of focal depths between 10 and 15 km. Although no clear planar geometries can yet be resolved from

the hypocenters, their distribution in groups 1 and 2 along with the hypocenter of the mainshock is consistent with a north-dipping (at 50°) fault plane, outcropping near the northern coast of Samos Island (Fig. 10, profile b_1-b_2, dashed line). The latter result is consistent with reported preliminary deformation observations, showing subsidence at the northern tip of Samos Island and mainly uplift to its western part (see Section 4.2).

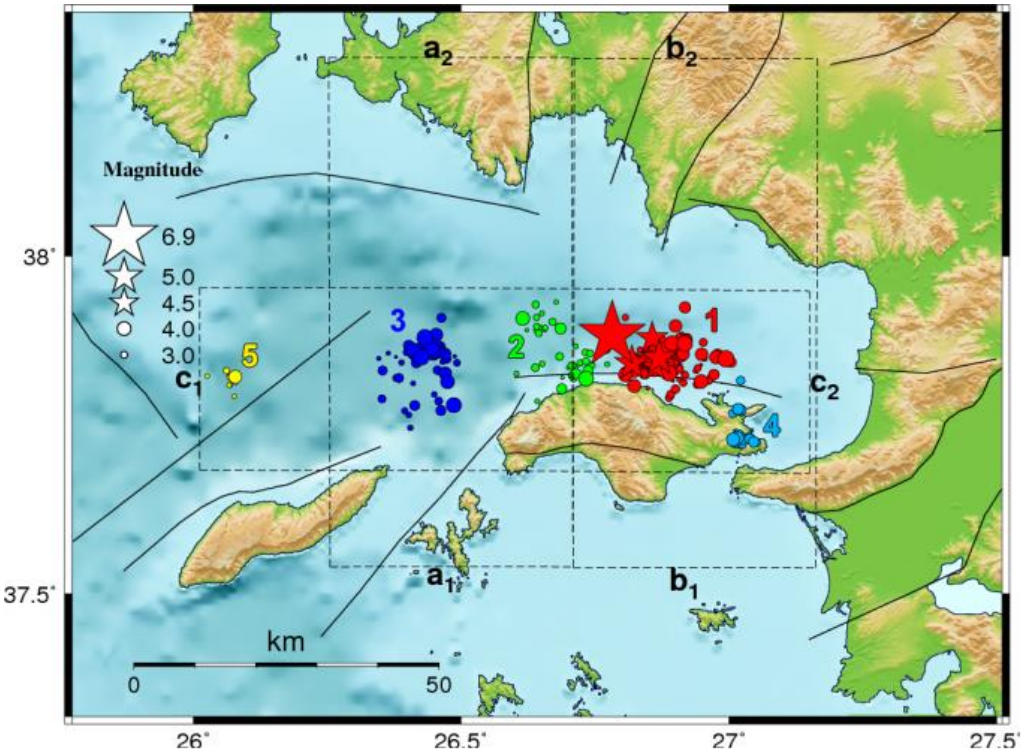

Fig. 9: Division of the 2020 Samos aftershocks into 5 distinct spatial groups (colours/number in the map). The major events with M≥4.5 are depicted by stars. Dashed rectangles with a-c labels represent the direction and limits for the cross-sections of Fig. 10.

The temporal evolution of the 2020 Samos aftershock sequence, until 8 November 2020, is presented in Fig. 11. Soon after the occurrence of the mainshock, the whole zone of groups 1-3 was activated, with most aftershocks occurring in group 1, east of the mainshock. During the first hours, the activity was limited to a total length of approximately 40 km (from 40 to 80 km in the vertical axis of Fig. 11), but as the sequence evolved it apparently gradually extended to ~60 km in the E-W direction. Group 4 (cyan) at the eastern part of Samos Island, notably south of the main aftershock zone, was activated on 31 October with a few events, while two distinct bursts occurred during 2-4 November 2020. The isolated group 5 (yellow) presented some activity on 3 and 6-7 November. No aftershocks with M≥4.5 were recorded after 31 October 2020. The activity of the aftershock sequence appears to be gradually diminishing, so far without any major secondary outbreak.

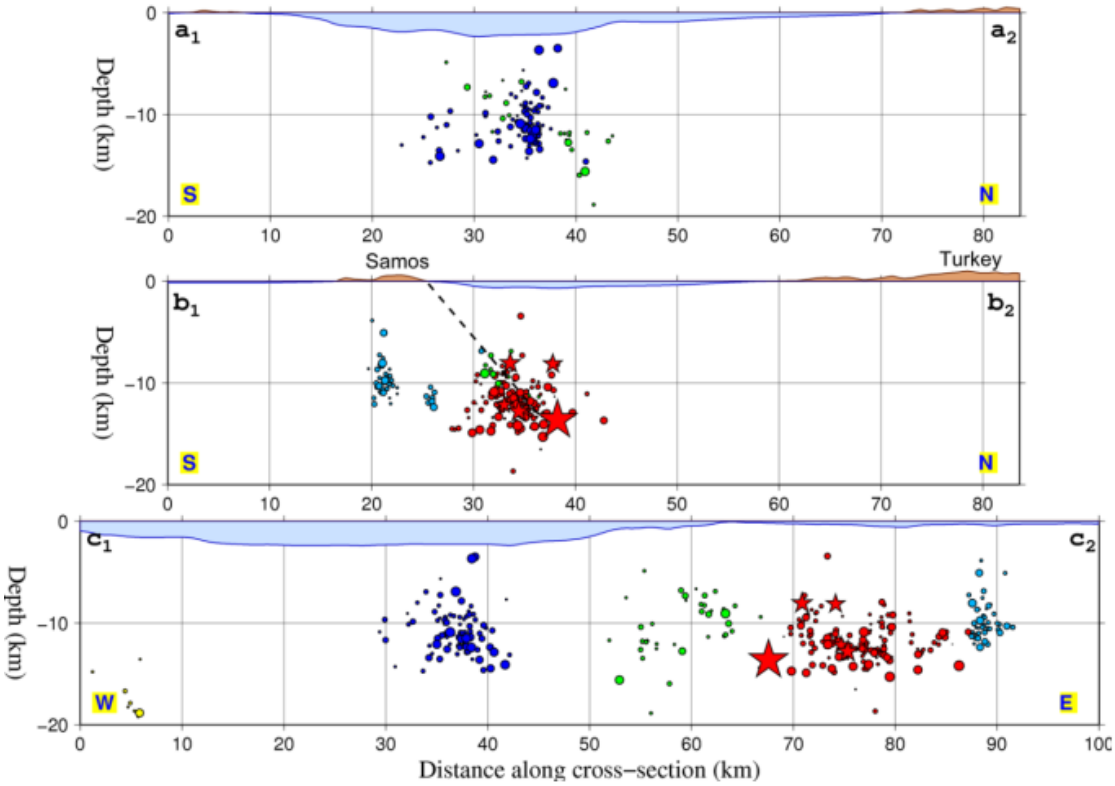

Fig. 10: Cross-sections in a S-N (a_1-a_2, b_1-b_2) and W-E direction (c_1-c_2) along the profiles presented by dashed rectangles on the map of Fig. 9. Topography and bathymetry at the top of the cross-sections have been vertically exaggerated by ×2. The major events with M ≥ 4.5 are depicted by stars.

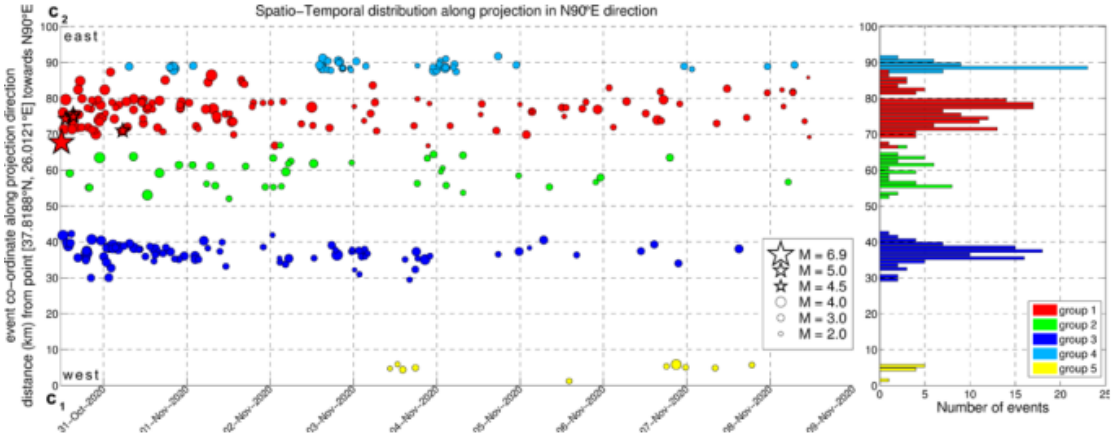

Fig. 11: Spatiotemporal projection of the 2020 Samos aftershocks epicenters along the W-E profile c_1-c_2 of Fig. 9. The histogram on the right shows the number of aftershocks along the profile. The major events with M ≥ 4.5 are depicted by stars.

4.4. Coulomb stress changes

Herein we present a preliminary model of the Coulomb Failure Function changes (ΔCFF) to examine the pattern of stress transfer due to the displacement caused by the M_w=6.9 mainshock. The ΔCFF model was determined using the Coulomb 3.3 software (Toda *et al.*, 2011), for a fault with a length (L) of 30 km and width (W) of 23 km, as well as a net slip (u) equal to 1,100 mm, with an effective coefficient of friction μ=0.4. This fault model is considered to cover the surface where the majority of coseismic slip has likely occurred, although different configurations may also be plausible (e.g. L=36 km, W=18 km; Ganas et al., 2020). The focal mechanism solution for the north-dipping nodal plane was considered (φ_1=270º, δ_1=50º, λ_1=-81º; Fig. 5) and the seismic moment magnitude of M_w=6.9. Fig. 12 presents the ΔCFF distribution for a horizontal slice of the model at a depth of 11 km, for receiver faults with the same kinematics as that of the mainshock. The Coulomb stress transfer distribution shows that the positive lobes (stress load; red) are spread to the west and to the east or the fault plane, while the negative lobes (stress shadow; blue) cover the regions to the north and to the south. This result indicates that, for the given configuration, the mainshock can trigger seismicity at the western and eastern edges of the main rupture surface. Even a simplified model such as this can explain the activity mainly at the western spatial group 3 (Fig. 9; blue), but also at the eastern ones (group 4 and most of group 1).

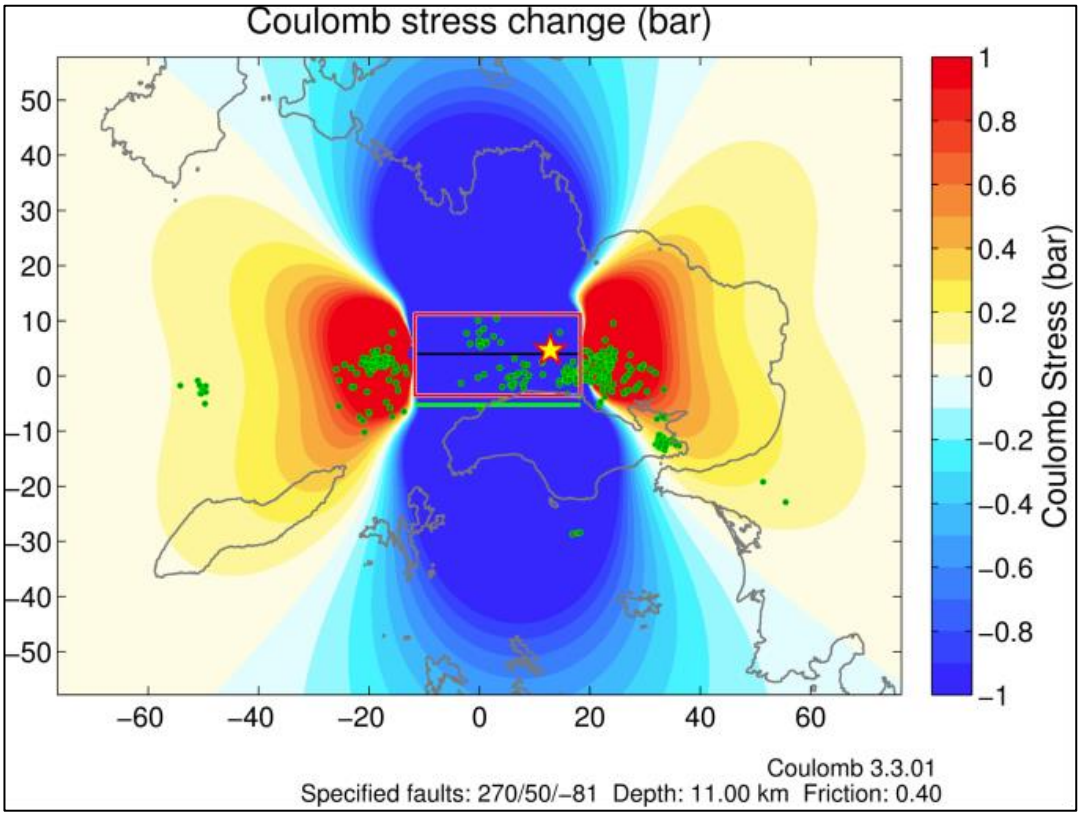

Fig. 12: ΔCFF values for receiver faults of similar kinematics as that of the mainshock at the depth of 11 km. The red rectangle shows the projection of the fault plane on the surface while the green line corresponds to the fault's trace when extrapolated to the surface. Red lobes indicate stress loading while blue regions depict stress shadows. The yellow star represents the mainshock and the green dots the epicenters of aftershocks from the relocated catalogue.

5. DISCUSSION AND CONCLUSIONS

The 2020 Samos earthquake was one of the strongest events to occur in Greece during the last decades, triggering the interest of geoscientists in Greece (e.g. Ganas *et al.*, 2020; Kalogeras *et al.*, 2020; Lekkas *et al.*, 2020; Papadimitriou *et al.*, 2020b; Triantafyllou *et al.*, 2020). However, considering its magnitude (M_w=6.9) and the fault's proximity to the island, Samos suffered relatively low damage compared to Izmir, located at a much greater distance of ~75 km from the mainshock's epicenter (Fig. 1). One of the main issues with such earthquakes, i.e. occurring offshore and exhibiting normal faulting, as was also the case of the 2017 Kos (Ganas *et al.*, 2019) or the 2017 Lesvos (Papadimitriou *et al.*, 2018) events, is the determination of the fault plane out of the two nodal planes of the focal mechanism. The deformation pattern (Fig. 7; see also Ganas *et al.*, 2020) greatly aids to resolve this ambiguity, as the preliminary results indicate that the western part of Samos Island was uplifted, while subsidence was observed at the northern edge of the central part of the island. Taking also into account the distribution of the relocated hypocenters (Fig. 10, b_1-b_2), a north-dipping fault plane can be inferred for the mainshock. This places most of Samos Island on the footwall, which is another factor that may have lowered the damage potential of the earthquake on the island.

ShakeMaps (USGS, 2017) depict the distribution and severity of ground shaking, information that is critical for assessing the extent of the areas affected, to determine which regions are potentially hit the hardest, allowing for a rapid estimation of losses. Fig. 13a presents the ShakeMap automatically generated for the 2020 Samos M_w=6.9 mainshock (more information is included in the event's dedicated webpage; http://www.geophysics.geol.uoa.gr/stations/gmaps3/eventpage_leaf.php?evid=2020-10-30-11-51-26&lng=en). The maximum observed intensity values reached VII at the northern part of Samos Island and the opposite coast of Turkey. To improve the ShakeMap, we also considered employing intensity data from testimonies of people who felt the earthquake. LastQuake (https://m.emsc.eu/) is a system that operates as a

junction among seismology, citizen science and digital communication. Its aim is to offer timely, appropriate information in regions where an earthquake has been felt and to collect high numbers of eyewitnesses' direct and indirect observations about the degree of shaking being felt and possible damage incurred (Bossu et al., 2018). This improves rapid situation awareness and augments data at low cost. The resulting intensities after the incorporation of LastQuake data (Fig. 13b) significantly increase with respect to the theoretically expected ones (Fig. 13a).

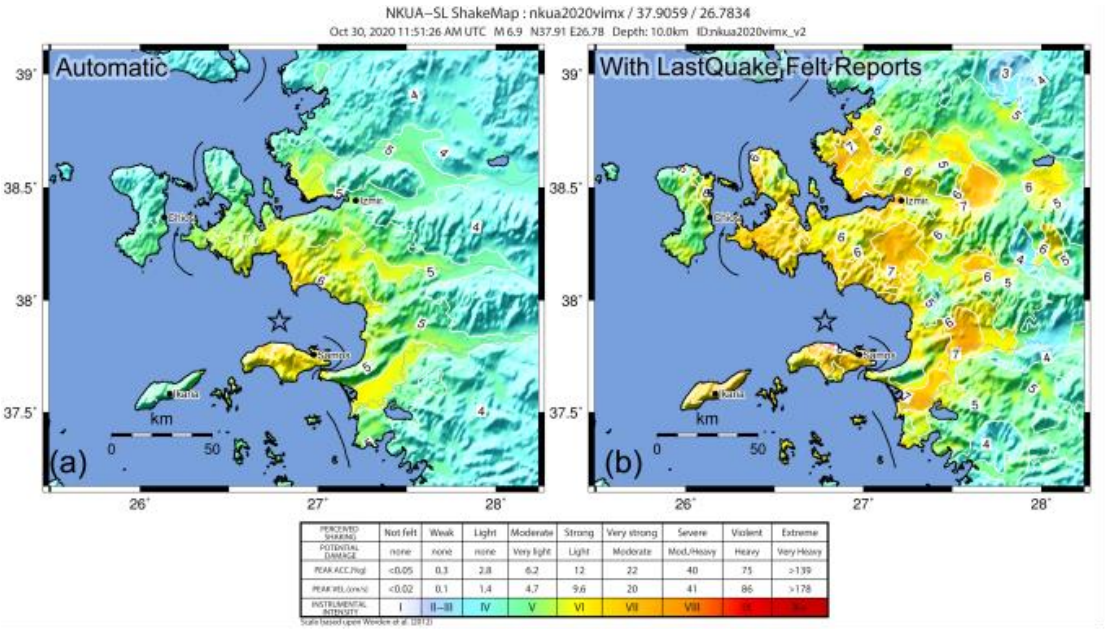

Fig. 13: (a) Automatically generated ShakeMap (USGS, 2017) for the 2020 Samos M_w=6.9 mainshock using ground motion prediction equations and V_{S30} theoretical estimates from topography through the Allen and Wald (2009) approach; (b) with additional information from the EMSC felt reports (https://m.emsc.eu/).

During the main seismic event of 30 October 2020, damage occurred to a number of structures, mainly old buildings and monumental structures (Papadimitriou *et al.*, 2020b). In general, considering the high intensity of the earthquake (Fig. 13) with Spectral Accelerations (SA) up to 0.6 g for periods within the 0.01-0.3 s range (ITSAK, 2020), the buildings on Samos Island behaved well. This range is close to the eigenperiod of most of the buildings, since over 99% of them have up to three storeys according to the 2011 building census data. The majority of the building stock in the island suffered minor damage, even though 70% of buildings were constructed before 1985, and thus, with low earthquake-resistant design (1959 seismic code) compared to the post-1985 codes, which includes EC8 (CEN, 2004). The overall satisfactory structural performance can be attributed to the good construction quality. Damage of

non-structural components was also evident in the areas of Samos Island with the highest observed intensities.

As far as the school buildings are concerned, until now, from the reports of the authorities, out of the 44 school units inspected, 11 have suffered extensive damage. It should be noted that most schools in Samos Island (about 80%) were constructed before 1985 and that only about 30% of school buildings are made from reinforced concrete. Some monumental structures, temples and churches also faced significant damages. More specifically, over 60 churches on the island were severely damaged by the earthquake. In the area of eastern Samos, 24 churches suffered significant damage. In west Samos, 30 churches were also damaged.

The acceleration response spectra of the recorded accelerations (www.itsak.gr) show that the high-rise buildings (4-6 storeys), were subjected to accelerations up to 1 g. This could be one of the reasons why the high-rise buildings in Izmir suffered more significant damages compared to the low to mid-rise buildings in Samos Island (Papadimitriou et al., 2020b). Of course, there are also other reasons, like the frequency content and the directivity of the excitations, the quality of the foundation soil, the constructions, etc. Additional acceleration measurements are presented in the report of Kalogeras *et al.* (2020).

A tsunami was generated by the Samos 2020 mainshock, producing minor damage at the surrounding coasts and especially in the towns of Vathy and Karlovasi in Samos Island (Greece; Triantafyllou et al., 2020) and Sigacik (Turkey) (Fig. 14). Water inundating through streets and ports in the region was reported in social media, along with tsunami warnings being issued for the Dodecanese islands in Greece. Heights of the tsunami from this event were larger than those of similar magnitude earthquakes in this region (Dağ, 2020). At the waterfront of Seferihisar, flooding reached heights of 1.9 m, causing one fatality; in Akarca, the tsunami reached heights of over 1 m, penetrating 0.8 km inland; in Azmak, the tsunami penetrated 1.3 km inland and in Sigacik 0.3 km (Dağ, 2020). More details about the impact of the tsunami are described in the report of Triantafyllou *et al.* (2020), while a preliminary numerical simulation of the tsunami is presented in the report of Kalogeras *et al.* (2020).

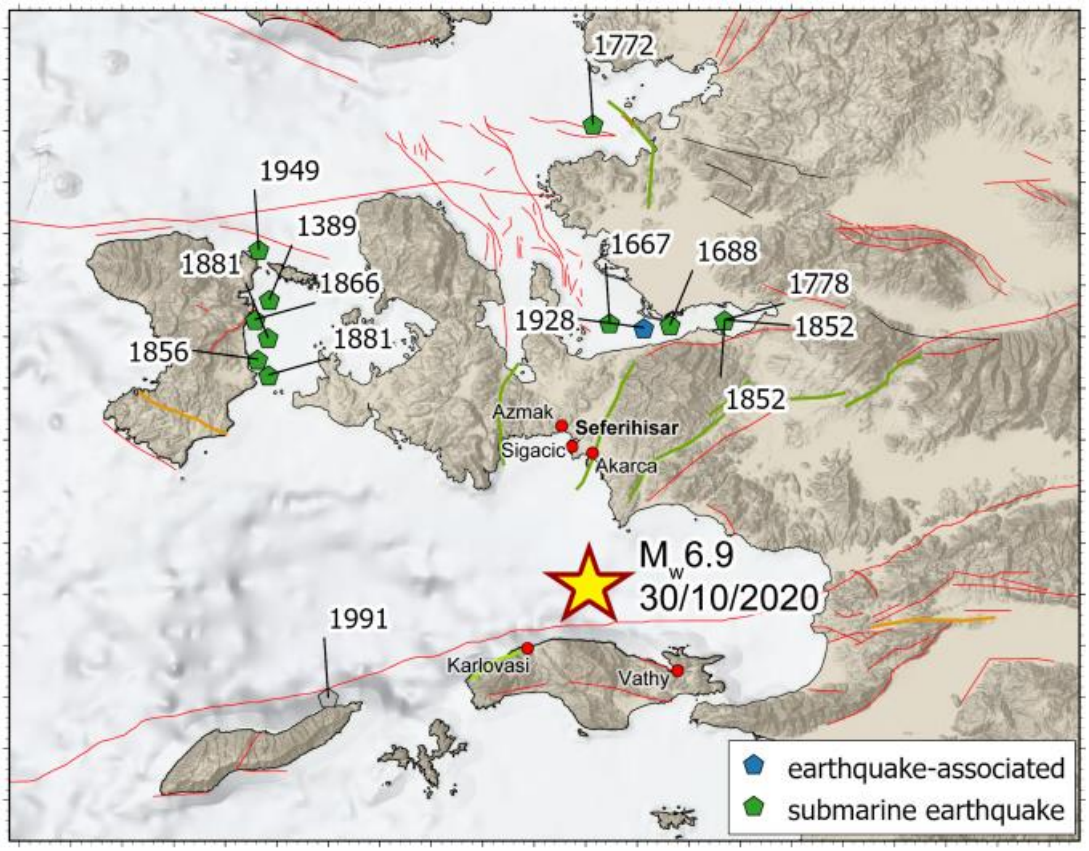

Fig. 14: Locations of tsunamis observed during the 30 October 2020 mainshock (red solid circles, Dağ, 2020; Triantafyllou et al., 2020). Historical tsunamis (solid polygons) observed in the epicentral area (Papadopoulos, 2001). Data and interactive map available at the New Seismotectonic Atlas of Greece (Kassaras *et al.*, 2020; http://www.geophysics.geol.uoa.gr/atlas.html)

The spatial distribution of hypocenters presents similarities with that of the 2017 Kos earthquake (Ganas *et al.*, 2019), in the sense that the eastern part of the aftershocks sequence was more densely populated with events than the western part, while a significant lack of aftershocks is observed between the two halves. This gap could coincide with the region of the fault surface where most of the co-seismic slip occurred, i.e. a large asperity that ruptured during the mainshock, thus only few aftershocks are observed therein (spatial group 2; Fig. 9). On the other hand, the Coulomb stress transfer pattern for this type of event and for receiver faults of similar kinematics (Fig. 12) shows that stress load is transferred to the eastern and western edges of the rupture plane. This can explain triggering of aftershocks in spatial groups 3 and 5 in the west (Fig. 9), but also group 4 in the eastern part of the island. The latter almost certainly belongs to a different fault than the one of the mainshock which could be related to some of the mapped structures observed on the island (Fig. 2).

The complex nature of this earthquake's source was indicated during our attempts to determine the mainshock's moment tensor. A more detailed investigation of its co-seismic slip model could reveal if a large asperity broke in the region where the gap in the aftershocks distribution is observed, as well as whether the mainshock ruptured more than one fault segments. The latter could explain why the largest aftershock is of the order of M_w=5.0 and not M_w≈6.0, as would be expected for a mainshock of M_w≈7.0, had it occurred on a single large fault.

6. ACKNOWLEDGEMENTS

We acknowledge support of this study by the project "HELPOS - Hellenic Plate Observing System" (MIS 5002697) which is implemented under the Action "Reinforcement of the Research and Innovation Infrastructure", funded by the Operational Programme "Competitiveness, Entrepreneurship and Innovation" (NSRF 2014-2020) and co-financed by Greece and the EU (European Regional Development Fund). We would like to thank the scientists and personnel who participated in the installation or maintenance of the permanent and temporary stations belonging to HUSN (HL, doi:10.7914/SN/HL; HT, doi:10.7914/SN/HT; HA, doi:10.7914/SN/HA; HP doi:10.7914/SN/HP; HI, doi:10.7914/SN/HI; HC, doi:10.7914/SN/HC) and KOERI (KO, doi:10.7914/SN/KO). Some maps were drawn using the Generic Mapping Tools (GMT) software (Wessel & Smith, 1998).

7. REFERENCES

Allen, T.I., Wald, D.J., 2009. On the Use of High-Resolution Topographic Data as a Proxy for Seismic Site Conditions (VS30). *Bull. Seismol. Soc. Am.*, 99, 935–943. https://doi.org/10.1785/0120080255

Ambraseys, N., 2009. Earthquakes in the Mediterranean and Middle East: a multidisciplinary study of seismicity up to 1900, *Cambridge University Press*, Cambridge. https://doi.org/10.1017/CBO9781139195430

Basili, R., Kastelic, V., Valensise, G., and DISS Working Group 2009 (2009), DISS3 tutorial series: Guidelines for compiling records of the Database of Individual Seismogenic Sources, version 3, Rapporti Tecnici INGV, no. 108, 20 p. Available at: http://diss.rm.ingv.it/diss/downloads/RT108.pdf (Last Accessed: 19 November 2020)

Benetatos, C., Kiratzi, A., Ganas, A., Ziazia, M., Plessa, A., Drakatos, G., 2006. Strike-slip motions in the Gulf of Sığaçik (western Turkey): Properties of the 17 October 2005

earthquake seismic sequence. *Tectonophysics* 426, 263–279. https://doi.org/10.1016/j.tecto.2006.08.003

Bossu, R., Roussel, F., Fallou, L., Landès, M., Steed, R., Mazet-Roux, G., Dupont, A., Frobert, L., Petersen, L., 2018. LastQuake: From rapid information to global seismic Risk reduction. *Int. J. Disaster Risk Reduct.*, 28, 32–42. https://doi.org/10.1016/j.ijdrr.2018.02.024

Bouchon, M., 1979. Discrete wave number representation of elastic wave fields in Three space dimension. *J. Geophys. Res.*, 84, 3609–3614. https://doi.org/10.1029/JB084iB07p03609

Bouchon, M., 2003. A review of the discrete wavenumber method. *Pure Appl. Geophys.*, 160, 445–465. https://doi.org/10.1007/PL00012545

CEN, 2004. Eurocode 8: Design of structures for earthquake resistance - Part 1: General rules, seismic actions and rules for buildings, European Standard EN 1998 1:2 004, Brussels, Belgium: European Committee for Standardisation.

Dağ, B., 2020. "Turkey sees larger tsunami after latest quake". *Anadolu Agency*. https://www.aa.com.tr/en/turkey/turkey-sees-larger-tsunami-after-latest-quake/2031162t (Last accessed: 27/11/2020)

Ganas, A., Tsironi, V., Kollia, E., Delagas, M., Tsimi, C., Oikonomou, A. 2018. Recent upgrades of the NOA database of active faults in Greece (NOAFAULTs). *19th General Assembly of WEGENER, September 2018, Grenoble*, sciencesconf.org:: 219400, https://doi.org/10.5281/zenodo.3483136

Ganas, A., Elias, P., Kapetanidis, V., Valkaniotis, S., Briole, P., Kassaras, I., Argyrakis, P., Barberopoulou, A., Moshou, A., 2019. The July 20, 2017 M6.6 Kos Earthquake: Seismic and Geodetic Evidence for an Active North-Dipping Normal Fault at the Western End of the Gulf of Gökova (SE Aegean Sea). *Pure Appl. Geophys.*, 176, 4177–4211. https://doi.org/10.1007/s00024-019-02154-y

Ganas, A., Elias, P., Briole, P., Tsironi, V., Valkaniotis, S., Escartin, J., Karasante, I., Efstathiou, E., 2020. Fault responsible for Samos earthquake identified. *Temblor*, http://doi.org/10.32858/temblor.134 (Last accessed: 19 November 2020)

Gasperini, P., Vannucci, G., Tripone, D., Boschi, E., 2010. The location and sizing of historical earthquakes using the attenuation of macroseismic intensity with distance. *Bull. Seismol. Soc. Am.*, 100, 2035–2066. https://doi.org/10.1785/0120090330

Genç, C.Ş., Altunkaynak, Ş., Karacık, Z., Yazman, M., Yılmaz, Y., 2001. The Çubukludağ graben, south of İzmir: its tectonic significance in the Neogene geological

evolution of the western Anatolia, *Geodin. Acta*, 14, 1-3, 45-55. https://doi.org/10.1016/S0985-3111(00)01061-5

Geoscope, 2020. Dodecanese Islands, Greece 2020/10/30 11:51:26 UTC, Mw=7.0 : http://geoscope.ipgp.fr/index.php/en/catalog/earthquake-description?seis=us7000c7y0 (Last Accessed: 25/11/2020)

Gürer, Ö.F., Sanğu, E., Özburan, M., Gürbüz, A., Sarica-Filoreau, N., 2013. Complex basin evolution in the Gökova Gulf region: implications on the Late Cenozoic tectonics of southwest Turkey. *Int. J. Earth Sci.*, 102, 2199–2221. https://doi.org/10.1007/s00531-013-0909-1

ITSAK, 2020. Earthquake North of Samos Island (Greece) of 30/10/2020-Preliminary Report, *ITSAK*, Thessaloniki pp. 9., report available at: http://www.itsak.gr/uploads/news/earthquake_reports/EQ_Samos_20201030_report_v2.pdf (Last accessed: 19 November 2020)

Jolivet, L., Brun, J.-P, 2010. Cenozoic geodynamic evolution of the Aegean. *Int. J. Earth Sci.*, 99, 109–138. https://doi.org/10.1007/s00531-008-0366-4

Kalogeras, I., Melis, N.S., Kalligeris, N., 2020. The earthquake of October 30th, 2020 at Samos, Eastern Aegean Sea, Greece. *Report published at EMSC*: https://www.emsccsem.org/Doc/Additional_Earthquake_Report/915787/Samos_Preminary_Report_EN.pdf (Last accessed: 19 November 2020)

Kapetanidis, V., Kassaras, I., 2019. Contemporary crustal stress of the Greek region deduced from earthquake focal mechanisms. *J. Geodyn.*, 123, 55–82. https://doi.org/10.1016/j.jog.2018.11.004

Karakonstantis, A., 2017. 3-D simulation of crust and upper mantle structure in the broader Hellenic area through Seismic Tomography. Ph.D. Thesis, Department of Geophysics-Geothermics, Faculty of Geology, University of Athens, Greece. (in Greek) http://hdl.handle.net/10442/hedi/40719 (Last Accessed: 27 November 2020)

Karakostas, V.G., Papadimitriou, E.E., Karakaisis, G.F., Papazachos, C.B., Scordilis, E.M. Vargemezis, G., Aidona, E., 2003. The 2001 Skyros, Northern Aegean, Greece, earthquake sequence: off-fault aftershocks, tectonic implications, and seismicity triggering. *Geophys. Res. Lett.*, 30(1), 1012. https://doi.org/10.1029/2002GL015814

Kassaras, I., Kapetanidis, V., Ganas, A., Tzanis, A., Kosma, C., Karakonstantis, A., Valkaniotis, S., Chailas, S., Kouskouna, V., Papadimitriou, P., 2020. The New Seismotectonic Atlas of Greece (v1.0) and Its Implementation. *Geosciences*, 10(11), 447. https://doi.org/10.3390/geosciences10110447

Kaviris, G., Papadimitriou, P., Kravvariti, P., Kapetanidis, V., Karakonstantis, A., Voulgaris, N., Makropoulos, K., 2015. A detailed seismic anisotropy study during the 2011–2012 unrest period in the Santorini Volcanic Complex. *Phys. Earth Planet. Inter.*, 238, 51–88. https://doi.org/10.1016/j.pepi.2014.11.002

Kissling, E., Ellsworth, W.L., Eberhart-Phillips, D., Kradolfer, U., 1994. Initial reference models in local earthquake tomography. *J. Geophys. Res.*, 99(B10), 19635-19646. https://doi.org/10.1029/93JB03138

Klein, F.W., 2002. User's guide to HYPOINVERSE-2000: a Fortran program to solve for earthquake locations and magnitudes, U.S. Geol. Surv. Prof. Pap., rep. 02-17, 1-123. https://doi.org/10.3133/ofr02171

Kouskouna, V., Sakkas, G., 2013. The University of Athens Hellenic Macroseismic Database (HMDB.UoA): historical earth- quakes. *J. Seismol.*, 17, 1253–1280. https://doi.org/10.1007/s10950-013-9390-3

Kurtuluş, C., Doğan, B., Sertçelik, F., Canbay, M., Küçük, H.M., 2009. Determination of the tectonic evolution of the Edremit Gulf based on seismic reflection studies. *Mar. Geophys. Res.*, 30, 121–134. https://doi.org/10.1007/s11001-009-9072-2

Lekkas, E., *et al.*, 2020. The October 30, 2020, Mw 6.9 Samos (Greece) earthquake. Newsletter of Environmental, Disaster, and Crises Management Strategies, Issue No. 21, November 2020, ISSN 2653-9454. Available at: https://edcm.edu.gr/en/newsletter/newsletter-21-the-october-30-2020-mw-69samosgreece-earthquake (Last Accessed: 19 November 2020)

Locati, M., Rovida, A., Albini, P., Stucchi, M., 2014. The AHEAD Portal: a gateway to European Historical Earthquake Data. *Seismol. Res. Lett.*, 85, 727–734.

https://doi.org/10.1785/0220130113

Makropoulos, K., Kaviris, G., Kouskouna, V., 2012. An updated and extended earthquake catalogue for Greece and adjacent areas since 1900. *Nat. Hazards Earth Syst. Sci.*, 12, 1425-1430. https://doi.org/10.5194/nhess-12-1425-2012

Malandri, C., Soukis, K., Maffione, M., Özkaptan, M., Vassilakis, E., Lozios, S., van Hinsbergen, D.J.J., 2017. Vertical-axis rotations accommodated along the Mid Cycladic lineament on Paros Island in the extensional heart of the Aegean orocline (Greece). *Lithosphere*, 9, 78–99. https://doi.org/10.1130/L575.1

Mascle, J., Martin, L., 1990. Shallow structure recent evolution of the Aegean Sea: a synthesis based on continuous reflection profiles. *Marine Geology*, 94, 271– 299. https://doi.org/10.1016/0025-3227(90)90060-W

McKenzie, D., 1972. Active tectonics of the Mediterranean region. *Geophys. J. Roy. Astr. Soc.*, 30(2),109-185. https://doi.org/10.1111/j.1365-246X.1972.tb02351.x

McKenzie, D., 1978. Active tectonics of the Alpine-Himalayan belt: the Aegean Sea and surrounding regions. *Geophys. J. R. Astr. Soc.*, 55, 217–254. https://doi.org/10.1111/j.1365-246X.1978.tb04759.x

Mercier, J.L., Sorel, D., Vergely, P., Simeakis, K., 1989. Extensional tectonic regimes in the Aegean basins during the Cenozoic. *Basin Research*, 2, 49-71. https://doi.org/10.1111/j.1365-2117.1989.tb00026.x

Ocakoğlu, N., Demirbağ, E., Kuşçu, İ., 2004. Neotectonic structures in the area offshore of Alaçatı, Doğanbey and Kuşadası (western Turkey): evidence of strike-slip faulting in the Aegean extensional province. *Tectonophysics*, 391(1-4), 67–83. https://doi.org/10.1016/j.tecto.2004.07.008

Papadimitriou, P., Chousianitis, K., Agalos, A., Moshou, A., Lagios, E., Makropoulos, K., 2012. The spatially extended 2006 April Zakynthos (Ionian Islands, Greece) seismic sequence and evidence for stress transfer. *Geophys. J. Int.*, 190, 1025–1040. https://doi.org/10.1111/j.1365-246X.2012.05444.x

Papadimitriou, P., Kapetanidis, V., Karakonstantis, A., Kaviris, G., Voulgaris, N., Makropoulos, K., 2015. The Santorini Volcanic Complex: A detailed multi-parameter seismological approach with emphasis on the 2011–2012 unrest period. *J. Geodyn.*, 85, 32–57. https://doi.org/10.1016/j.jog.2014.12.004

Papadimitriou, P., Kassaras, I., Kaviris, G., Tselentis, G.-A., Voulgaris, N., Lekkas, E., Chouliaras, G., Evangelidis, C., Pavlou, K., Kapetanidis, V., Karakonstantis, A., Kazantzidou-Firtinidou, D., Fountoulakis, I., Millas, C., Spingos, I., Aspiotis, T., Moumoulidou, A., Skourtsos, E., Antoniou, V., Andreadakis, E., Mavroulis, S., Kleanthi, M., 2018. The 12th June 2017 M_w = 6.3 Lesvos earthquake from detailed seismological observations. *J. Geodyn.*, 115, 23–42. https://doi.org/10.1016/j.jog.2018.01.009

Papadimitriou, P., Kapetanidis, V., Karakonstantis, A., Spingos, I., Pavlou, K., Kaviris, G., Kassaras, I., Sakkas, V. Voulgaris, N., 2020a. The 25 October, 2018 Zakynthos (Greece) earthquake: seismic activity at the transition between a transform fault and a subduction zone, *Geophys. J. Int.*, GJI-19-0844. (*submitted*)

Papadimitriou, P., Kapetanidis, V., Karakonstantis, A., Spingos, I., Kassaras, I., Sakkas, V., Kouskouna, V., Karatzetzou, A., Pavlou, K., Kaviris, G. & Voulgaris, N., 2020b. Preliminary report on the Mw=6.9 Samos earthquake of 30 October 2020. *Report released to EMSC-CSEM*. Available online at:

https://www.emsccsem.org/Doc/Additional_Earthquake_Report/915787/Samos2020_preliminary-report_nkua.pdf (Last accessed: 19 November 2020)

Papadopoulos, G.A., 2001. Tsunamis in the east Mediterranean: 1. A catalogue for the area of Greece and adjacent seas. In: *proceedings of the "Joint IOC – IUGG International Workshop: Tsunami Risk Assessment Beyond 2000: Theory, Practice and Plans, Moscow, June 14-16, 2000"*, pp. 34-43.

Papazachos, B.C., Papazachou, C., 2003. The earthquakes of Greece, Ziti Publ Co, Thessaloniki, Greece.

Pomonis, P., Hatzipanagiotou, K., 1998. Petrography and geochemistry of relict peridotites of the Kallithea-Drakei area (W. Samos). *Bul. Geol. Soc. Greece*, 32, 215-224.

Ring, U., Okrusch, M., Will, T. 2007. Samos Island, Part I: metamorphosed and non metamorphosed nappes, and sedimentary basins. In: Lister, G., Forster, M., Ring, U. (Eds.), *Inside the Aegean Metamorphic Core Complexes, Journal of the Virtual Explorer*, Electronic Edition, ISSN 1441-8142, volume 27, paper 5. https://doi.org/10.3809/jvirtex.2007.00180

Roumelioti, Z., Kiratzi, A., Melis, N., 2003. Relocation of the 26 July 2001 Skyros Island (Greece) earthquake sequence using the double-difference technique. *Phys. Earth Planet. Inter.*, 138(3-4), 231–239. https://doi.org/10.1016/S0031-9201(03)00138-9

Stucchi, M., Rovida, A., Gomez Capera, A.A., Alexandre, P., Camelbeeck, T., Demircioglu, M.B., Gasperini, P., Kouskouna, V., Musson, R.M.W., Radulian, M., Sesetyan, K., Vilanova, S., Baumont, D., Bungum, H., Fäh, D., Lenhardt, W., Makropoulos, K., Martinez Solares, J.M., Scotti, O.,Zivcic, M., Albini, P., Batllo, J., Papaioannou, C., Tatevossian, R., Locati, M., Meletti, C., Viganò, D., Giardini, D., 2013. The SHARE European Earthquake Catalog (SHEEC) 1000–1899. *J. Seismolog.*, 17 (2), 523–544. https://doi.org/10.1007/s10950-012-9335-2

Tan, O., Papadimitriou, E.E., Pabucçu, Z., Karakostas, V., Yörük, A., Leptokaropoulos, K., 2014. A detailed analysis of microseismicity in Samos and Kusadasi (Eastern Aegean Sea) areas. *Acta Geophys.*, 62, 1283–1309. https://doi.org/10.2478/s11600-013-0194-1

Taxeidis K., 2003. Study of Historical Seismicity of the Eastern Aegean Islands, PhD thesis, National and Kapodistrian University of Athens, Greece, 301 pp.

Toda, S., Stein, R.S., Sevilgen, V., Lin, J., 2011. Coulomb 3.3 Graphic-rich deformation and stress-change software for earthquake, tectonic, and volcano research and teaching-

user guide. U.S. Geological Survey Open-File Report 2011-1060, pp. 63. http://pubs.usgs.gov/of/2011/1060/ (Last Accessed: 27 November 2020)

Triantafyllou, I., Gogou, M., Mavroulis, S., Katsetsiadou, K.-N., Lekkas, E., Papadopoulos, G.A., 2020. The tsunami caused by the 30 October 2020 Samos (Greece), East Aegean Sea, Mw6.9 earthquake: impact assessment from post-event field survey and video records. Report published at EMSC: https://edcm.edu.gr/images/docs/2020/Samos2020-TSUNAMI-REPORT.pdf (Last Accessed: 19 November 2020)

USGS, 2017. ShakeMap – Earthquake Ground Motion and Shaking Intensity Maps: U.S. Geological Survey, https://doi.org/10.5066/F7W957B2.

USGS, 2020. M 7.0 - 15 km NNE of Néon Karlovásion, Greece: https://earthquake.usgs.gov/earthquakes/eventpage/us7000c7y0/finite-fault (Last Accessed: 25 November 2020)

Vavryčuk, V., 2014. Iterative joint inversion for stress and fault orientations from focal mechanisms. *Geophys. J. Int.*, 199, 69–77. https://doi.org/10.1093/gji/ggu224

Waldhauser, F., 2001. HypoDD-A Program to Compute Double-Difference Hypocenter Locations, U.S. Geol. Surv. Open File Rep. 01-113, 25 p. Wessel, P., Smith, W.H.F., 1998. New, improved version of generic mapping tools released, *Eos. Trans. Am. Geophys. Union*, 79, 579. https://doi.org/10.1029/98EO00426

Woessner, J., Danciu, L., Giardini, D., Crowley, H., Cotton, F., Grünthal, G., Valensise, G., Arvidsson, R., Basili, R., Demircioglu, M.B., Hiemer, S., Meletti, C., Musson, R.W., Rovida, A.N., Sesetyan, K., Stucchi M. and the SHARE Consortium, 2015. The 2013 European Seismic Hazard Model: key components and results. *Bull Earthquake Eng.*, 13, 3553–3596. https://doi.org/10.1007/s10518-015-9795-1